



Effect of Water Infiltration, Injection Rate and Anisotropy on Hydraulic Fracturing Behavior of Granite

Li Zhuang¹ · Kwang Yeom Kim¹ · Sung Gyu Jung² · Melvin Diaz² · Ki-Bok Min³

Received: 30 July 2017 / Accepted: 4 February 2018 / Published online: 14 February 2018
© The Author(s) 2018. This article is an open access publication

Abstract

Hydraulic fracturing tests on Pocheon granite cylinders at seven different injection rates varying from 1 to 100 mm³/s were conducted. They were compared with sleeve fracturing tests in which borehole was sleeved, and therefore, water infiltration influence was excluded. Hydraulic fracturing behavior of granite is significantly influenced by water infiltration, which is closely related to the preexisting microcracks in granite as well as the cleavage anisotropy. There was a threshold injection rate to fracture the granite specimen under given stress conditions. When the injection rate is below the threshold, water infiltrated granite matrix with slow increment of injection pressure, and the specimen finally reached a full saturation without fracturing. Injection pressure developed nonlinearly with time during water infiltration, while approximately linearly when infiltration was excluded. For both hydraulic and sleeve fracturing tests, breakdown pressure increases with increasing injection rate. The breakdown pressures by sleeve fracturing were more than two times higher than those in hydraulic fracturing. X-ray computed tomography (CT) observations show that induced fractures are along the weaker cleavage parallel to the direction of the vertical stress. The higher breakdown pressure results in a larger aperture of fractures in hydraulic fracturing tests.

Keywords Hydraulic fracturing · Sleeve fracturing · Injection rate · Water infiltration · Anisotropy · CT image

1 Introduction

Hydraulic fracturing behavior of various rocks such as sandstones, shales, granites and even artificial rocks has been widely studied over a period of years. Hydraulic fracturing tests in laboratory are usually carried out under constant injection rate or pressurization rate, and the breakdown pressure observed from the laboratory tests was found to be loading rate dependent. However, there was no consistent conclusion on the rate-dependent influence. Some reported an increase in breakdown pressure with increasing injection or pressurization rate in hydrostone (Haimson and Fairhurst

1969), Weber and Ruhr sandstones (Zoback et al. 1977), granite (Solberg et al. 1980), cement and mortar (Ha et al. 2017) and clay shale (Morgan et al. 2017), while some others reported an opposite finding in tight gas sandstone (Zeng and Roegiers 2002). Solberg et al. (1977) reported there is no difference in breakdown pressures of granite specimens at very slow injection rates of 0.33–3.3 mm³/s. It has been argued that pressurization rate influences the breakdown pressure depending upon whether the rock is permeable or not (Zoback et al. 1977, Detournay and Cheng 1992; Garagash and Detournay 1996). Clearly, the loading rate-dependent phenomena are related to the infiltration of injecting fluids in different rocks. A few studies performed sleeve fracturing tests to exclude hydraulic effects (Ishida et al. 1997; Brenne et al. 2013; Stoeckert et al. 2015).

Various theoretical models or equations have been presented to predict breakdown pressure of rocks during hydraulic fracturing. Guo et al. (1993) systematically reviewed several typical models including the first breakdown model by Hubbert and Willis (1957), tensile strength model, poroelastic model, shear failure model, point stress model and fracture mechanics model. They concluded that most of the models have their own limitation, and the

✉ Kwang Yeom Kim
kimky@kict.re.kr

¹ Korea Institute of Civil Engineering and Building Technology, 283 Goyangdae-ro, Ilsanseo-gu, Goyang 10223, Korea

² University of Science and Technology, 217 Gajeong-ro, Yuseong-gu, Daejeon 34113, Korea

³ Department of Energy Resources Engineering and Research Institute of Energy and Resources, Seoul National University, Gwanak-ro 599, Gwanak-gu, Seoul 08826, Korea

fracture mechanics model is the most promising one which is possible to explain phenomenon of rate, size, fracture fluid and stress dependent. The main difficulty in predicting breakdown pressure is that injected fluid penetrates into rock matrix and complicates the breakdown process. Stress changes induced by the fluid infiltration in rocks especially in low-permeability rocks and their influence on fractures development have not been fully understood yet.

Pioneering experimental and theoretical work considering penetration of injected fluid during hydraulic fracturing has been conducted by Haimson and Fairhurst (1967, 1969, 1970), Haimson (1968, 1975). The model presented by Haimson and Fairhurst (H–F model) (1967) introduced the Biot's poroelastic parameter when analyzing stresses in rock. Later Detournay and Cheng (1992) introduced a length-scale parameter around the wellbore in their breakdown model (D–C model) where fluid diffusion along the length was considered. Degue and Ladanyi (2000) also mentioned that the effect of pressurization rate on the breakdown pressure is closely related to the extent of fluid penetration into the cracks. Song and Haimson (2001) modified the D–C model by replacing the Terzaghi's effective stress with a general effective stress based on experimental results of high-porosity (26%) Tablerock sandstone.

Hydraulic fracturing behavior of different granites has been reported by Haimson (1975, 1999), Haimson and Lee (1980), Solberg et al. (1980), Haimson and Doe (1983), Haimson and Zhao (1991), Zhao et al. (1996), Ishida et al. (1997, 2000, 2004, 2012) and Chen et al. (2015). However, in these studies granites were mainly treated as low-permeability rocks and the influence of infiltration of injection fluid has rarely been discussed. Moreover, there is anisotropy phenomenon in some granites and they have three cleavages or planes of weakness called rift, grain and hardway (Douglass and Voight 1969; Fujii et al. 2007). The cleavages have different tensile strength and permeability and therefore influence fracture generation in laboratory hydraulic fracturing test (Chen et al. 2015; Zhuang et al. 2016a; Diaz et al. 2016).

Geometrical properties including the aperture of induced fractures are very important for deep geothermal energy development in crystalline rocks. For measurement of the aperture of fractures, X-ray computed tomography (CT) as a nondestructive method was often used (Johns et al. 1993; Keller 1997; Bertels et al. 2001; Zhuang et al. 2016a). This method can help to analyze geometric properties of induced fractures as well as fracture propagation (Renard et al. 2009; Jia et al. 2013; Li et al. 2017). Large apertures can be measured directly by counting the number of pixels across the fracture width while measurement on small apertures less than 1 pixel requires a special approach (Keller 1997).

In this study, hydraulic fracturing and sleeve fracturing tests on granite samples were both performed under seven different injection rates and test results were compared to

clarify the influence of water infiltration. X-ray computed tomography (CT) was applied to analyze preexisting microcracks and induced fractures in granite specimens.

2 Experimental Setup

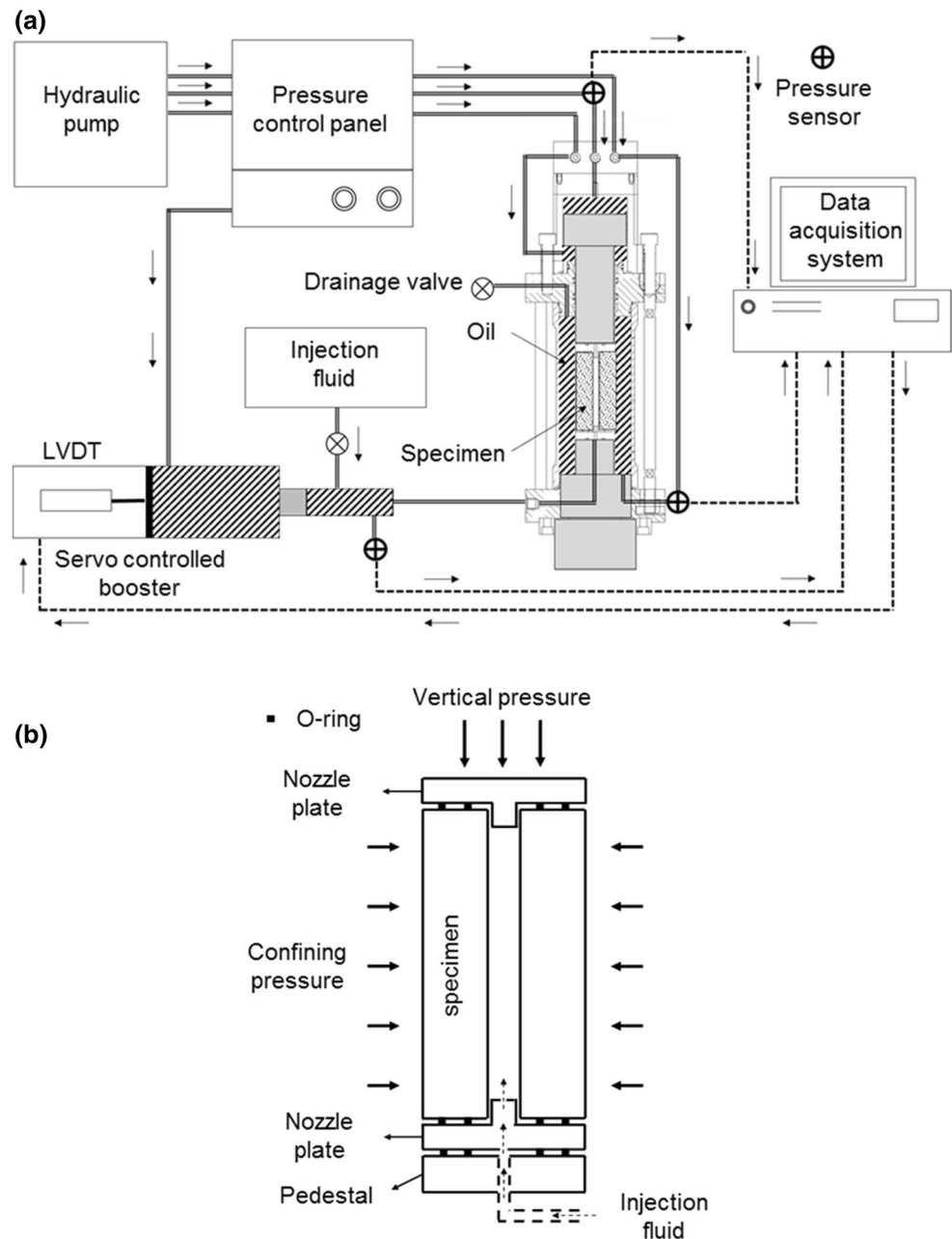
2.1 Test Equipment

We developed a hydraulic fracturing test equipment for core-scale samples (Fig. 1). One chamber covered the testing section around the specimen to apply hydrostatic pressure on test specimen. The specimen was connected to the top and bottom nozzle plates. O-rings were installed inside nozzle plates to prevent water and pressure leakage. A membrane was placed around the specimen, and therefore, it was isolated from oil in the chamber in case of a confining pressure being applied. Fluid was injected into specimen from the bottom at a constant injection rate or pressurization rate through a servo-controlled injecting system. The maximum injection pressure is 35 MPa, and the maximum confining pressure is 20 MPa. Four pressure sensors were installed. Two of them were used to measure injection fluid pressures near the specimen and near the booster, and the other two were used to measure confining pressure in the cell and vertical pressure in the upper chamber. Displacement of booster was measured by a LVDT (linear variable differential transformer), and therefore, injection rate can be estimated based on the displacement per unit time and the cross-sectional area of the booster.

2.2 Rock Sample

Test material was Pocheon granite taken from Pocheon area in Korea. X-ray diffraction analysis shows that the granite is largely composed of albite (35.9%), quartz (35.7%), microcline (25.8%) and biotite (2.6%). The average measured effective porosity is 0.66%. The Pocheon granite shows mild but clear anisotropy with three typical cleavages of rift (R), grain (G) and hardway (H). The measured average grain size is 0.94 mm in rift plane, 1.01 mm in grain plane and 0.91 mm in hardway plane. Among the three planes, rift plane has the highest microcrack density and therefore its tensile strength is the lowest, whereas the hardway plane has the lowest microcrack density and the highest tensile strength (Park et al. 2004; Zhuang et al. 2016b). Figure 2a, b shows microcracks in a thin section of Pocheon granite cut parallel to the rift plane. Both of intergranular and transgranular microcracks exist, and most of these microcracks were found in quartz grains. Park et al. (2004) reported that the preferred orientation of transgranular microcracks in the quartz is approximately parallel to the rift plane. Figure 2c, d shows a very small granite sample with diameter of 5 mm

Fig. 1 Schematic diagram of the hydraulic fracturing test system: **a** overview and **b** details around the specimen. Linear variable displacement transducer (LVDT)



and a three-dimensional CT image of microcracks extracted from the sample with the voxel pitch of 8 μm . It is observed that each microcrack is a plane and some planes connect in the three-dimensional spatial distribution.

Granite specimens were cored in directions perpendicular to the three cleavage planes, and their basic physical and mechanical properties were measured. Table 1 lists main measured results. Elastic modulus was measured on cylinders having diameters of 50 mm and lengths of 200 mm. Brazilian tensile strength (BTS) was measured with disks having diameters of 50 mm and thicknesses of 25 mm, and the loading direction was parallel to the rift,

grain and hardway plane, respectively. Uniaxial compressive strength (UCS) was measured with cylinders having diameters of 50 mm and heights of 100 mm. Hydraulic conductivity was measured with cylinders having diameters of 50 mm and heights of 50 mm at a water temperature of 15 $^{\circ}\text{C}$ and a constant water head pressure of 0.1 MPa. Figure 3 shows the three typical specimens used in fracturing tests, and they were labeled with R, G and H, respectively. Each specimen is 50 mm in diameter and 100 mm high. The diameter of a through-going borehole in the center of specimen is around 8 mm.

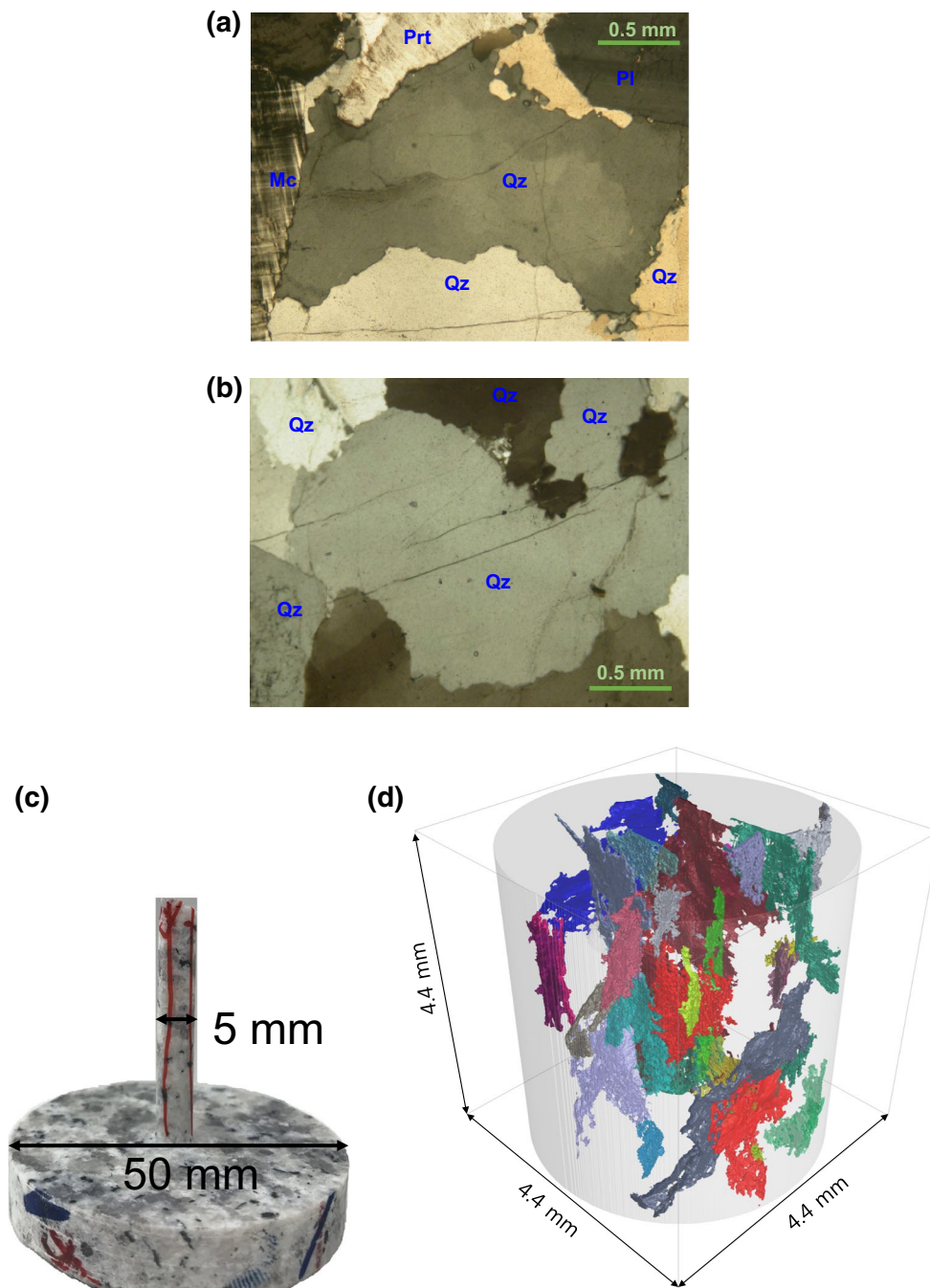


Fig. 2 Preexisting microcracks in granite. **a, b** Thin sections of Pocheon granite cut parallel to the rift plane. Major microcracks were found in quartz grains. *Qz* quartz, *Mc* microcline, *Pl* plagioclase,

Prt perthite, **c** a mini granite sample with diameter of 5 mm and **d** 3D spatial distribution of microcracks, the colors represent different microcracks

2.3 Test Conditions

The confining pressure was selected to be zero for all of the tests in this study, and the influence of confining pressure is not considered. The vertical pressure was fixed to be around 25 MPa to make sure of safe sealing and no leakage from the top and bottom surfaces of specimen connecting with

nozzle plates. Due to the above stress conditions, vertical tensile hydraulic fractures will be induced in the samples.

Hydraulic fracturing tests used H and R specimens. G specimen was not used because it was tested to have similar hydraulic fracturing behavior with H specimen because they have the same weak plane of the rift in radial direction. Injection rate was constant in each test, and seven different

Table 1 Main physical and mechanical parameters of Pocheon granite

Specimen/plane	Dry density (g/cm ³)	Hydraulic conductivity* (m/s)	Elastic modulus** (GPa)	BTS*** (MPa)	UCS** (MPa)	Toughness*** (MPa m ^{1/2})
Rift (R)	2.609	1.09E-10	57.53	6.05	220.01	0.963
Grain (G)		8.34E-11	55.09	8.20	194.62	1.211
Hardway (H)		7.20E-11	58.47	8.83	192.10	1.583

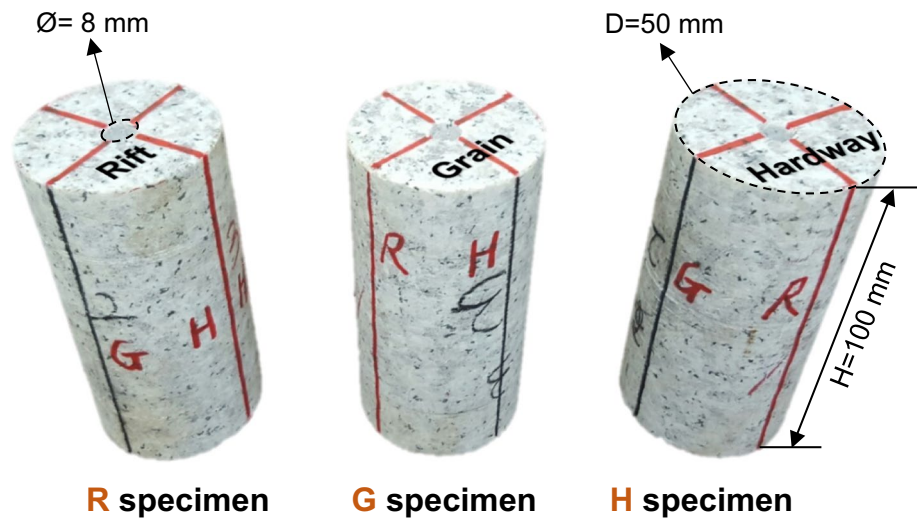
Hydraulic conductivity, BTS and toughness were measured along the rift, grain and hardway planes. Elastic modulus and UCS were measured on the R, G and H specimens

*Averaged by 3 testing values

**Averaged by 5 testing values

***Averaged by 20 testing values

Fig. 3 Granite specimens cored in directions perpendicular to the rift, grain and hardway planes. \varnothing borehole diameter, D sample diameter, H sample height



injection rates were used ($q = 1, 5, 10, 25, 50, 75,$ and $100 \text{ mm}^3/\text{s}$). The highest injection rates were chosen referring to past studies using similarly sized specimens (Solberg et al. 1980; Brenne et al. 2013). Sleeve fracturing tests were performed on H specimens for comparison with hydraulic fracturing tests. The borehole, top surface and bottom surface were sleeved with a latex cover to prevent water infiltration. The main test conditions are summarized in Tables 2 and 3. Moreover, injection tests without fracturing were performed on additional granite specimens to measure how much water infiltrates into specimen at different injection time and injection pressures.

3 Experimental Results and Analysis

3.1 Influence of Injection Rate

Figure 4 plots injection pressure with respect to total injected volume of H specimens under the seven different injection

rates from 1 to $100 \text{ mm}^3/\text{s}$. The volume is calculated as the injection rate (q) multiplied by injection time (t). The x -axis gives the total injected volume instead of injection time because the total injection time spent at the end of test for the lowest and the highest injection rate are very different and it is difficult to view each result clearly in the same scale of time. It should be noted that the total injected volume does not mean the volume of water infiltrating into specimen, as some water discharged through outside surface of cylinder. The beginning section of each curve shows a slow increase in injection pressure because there was air remained in the booster, which delayed compression of the water to provide pressure.

Two types of curve pattern are observed in the figure. The first type presents at low injection rates from 1 to $25 \text{ mm}^3/\text{s}$. Injection pressure increased slowly with increasing injected volume and then converged to a certain value, which is defined as the maximum injection pressure P_{max} . A peak injection pressure was not observed, which indicates that the specimen was not hydrofractured. The second type presents

Table 2 Test conditions and main results of hydraulic fracturing tests

Specimen	Pumping rate (mm ³ /s)	Resultant pressurization rate (MPa/s)	Breakdown pressure (MPa)	Max. injection pressure (MPa)	Max. aperture of fractures (pixel)
H specimen	1	2×10^{-4}	–	0.78	No fractures
	5	0.003	–	1.59	No fractures
	10	0.016	–	3.11	No fractures
	25	0.074	–	5.79	< 1
	50	0.218	6.00	–	4
	75	0.265	6.50	–	5
	100	0.609	7.42	–	6
R Specimen	1	1×10^{-4}	–	0.71	No fractures
	5	0.003	–	2.04	No fractures
	10	0.029	–	4.17	No fractures
	25	0.130	7.17	–	3
	50	0.366	8.14	–	6
	75	0.343	7.93	–	8
	100	0.518	8.38	–	8

The confining pressure was 0, and the vertical pressure was around 25 MPa in all of the tests

1 pixel = 0.0569 mm

Table 3 Test conditions and main results of sleeve fracturing tests

Specimen	Pumping rate (mm ³ /s)	Resultant pressurization rate (MPa/s)	Breakdown pressure (MPa)	Max. aperture of fractures
H specimen	1	0.009	18.49	Unmeasurable (split in two)
	5	0.040	20.10	
	10	0.099	19.66	
	25	0.253	19.73	
	50	0.608	21.12	
	75	0.702	20.78	
	100	1.316	22.42	

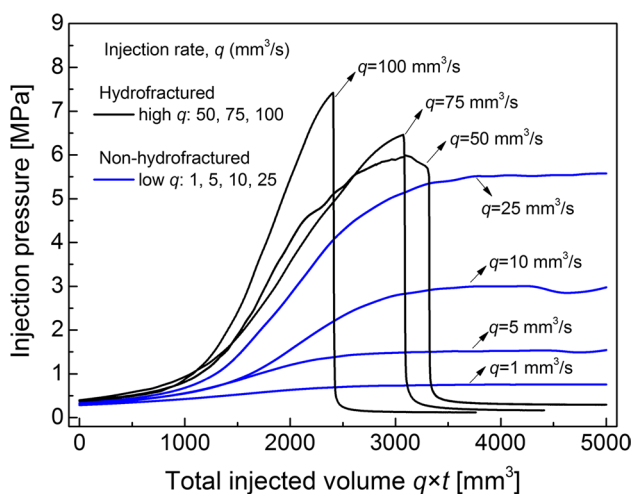


Fig. 4 Injection pressure plotted with respect to total pumped volume at different injection rates for H specimens. The total pumped volume was estimated by multiplying the pumping time t by the injection rate q

at high injection rates from 50 to 100 mm³/s. Injection pressure increased faster compared to those at low injection rates and reached a peak called breakdown pressure (P_b). After the peak, injection pressure dropped very quickly to zero because the confining pressure was zero. For both types of curves, the ascending section was not linear especially when approaching P_{max} or P_b .

3.2 Measurement of Water Infiltration

To explain the two types of injection pressure variation and also to further investigate the effect of water infiltration, additional injection tests were performed to measure the weight of water infiltrated into granite specimen at different time and different resultant injection pressures. To avoid any influence of water injection, each specimen was used only once. Specimens were completely dried and weighed before testing. Water was injected at a constant injection rate and injection was stopped when the injection pressure reached

a certain value. The specimen was removed and weighed again. The remained water adhered to the surface and borehole was blown off with a drier. The difference between the initial weight and the weight after testing is attributed to the weight of water infiltrated into the specimen during injection. The total volume of interconnected pores was estimated as the average effective porosity (0.66%) multiplied by the volume of the specimen. The ratio of volume of infiltrated water and the total volume of pores is defined as degree of saturation.

Figure 5a, b compares variations of injection pressure and degree of saturation at a low injection rate of $1 \text{ mm}^3/\text{s}$ and a high injection rate of $100 \text{ mm}^3/\text{s}$. At the low injection rate of $1 \text{ mm}^3/\text{s}$, the specimen reached full saturation after 2000 s while the injection pressure was only 0.45 MPa. Given that the specimen was saturated, inflow and outflow reach equilibrium and injection pressure will not increase any more. As a result, specimen was not hydrofractured. At the high

injection rate of $100 \text{ mm}^3/\text{s}$, degree of saturation was $< 80\%$ while the injection pressure almost reached the breakdown pressure, meaning that specimen was fractured before it was fully saturated. In the same way, for injection tests at low injection rates of 10 and $25 \text{ mm}^3/\text{s}$, the maximum injection pressures were only 2.06 and 5.06 MPa as full saturation is approached. As a result, the specimens were not hydrofractured because the injection pressures are much lower than the threshold breakdown pressure (around 6.0 MPa). At the injection rate of $50 \text{ mm}^3/\text{s}$, breakdown was achieved at a degree of saturation around 80%.

3.3 Influence of Rock Anisotropy

Granite shows mild but clear anisotropy along three typical cleavage planes with different microcrack densities and thus with different tensile strength and hydraulic conductivities. The anisotropy therefore influences hydraulic

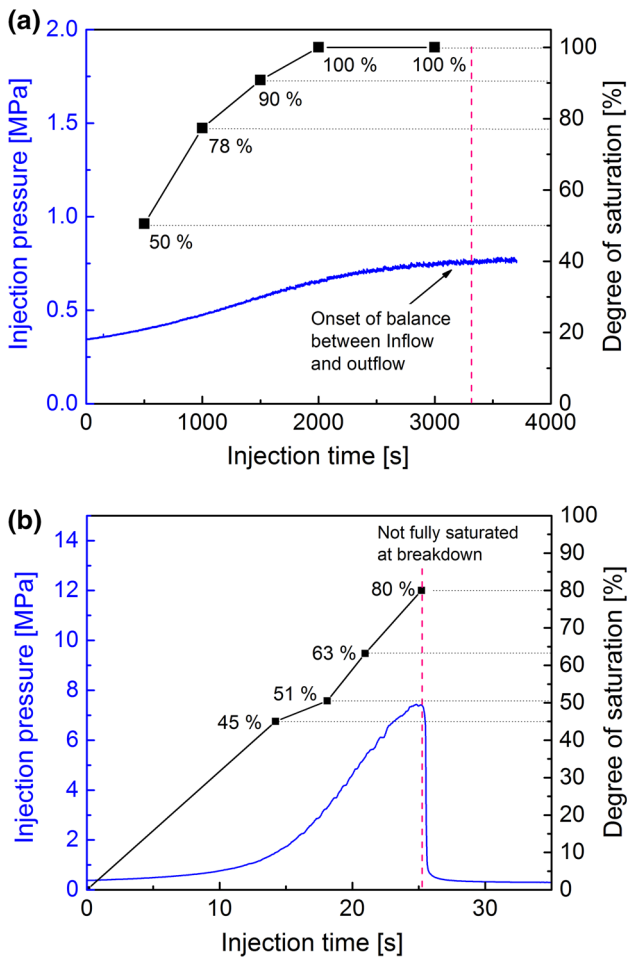


Fig. 5 Injection pressure and degree of saturation with respect to injection time. **a** Injection rate $q = 1 \text{ mm}^3/\text{s}$ and **b** $q = 100 \text{ mm}^3/\text{s}$. P_{max} is the maximum injection pressure at the end of each injection test

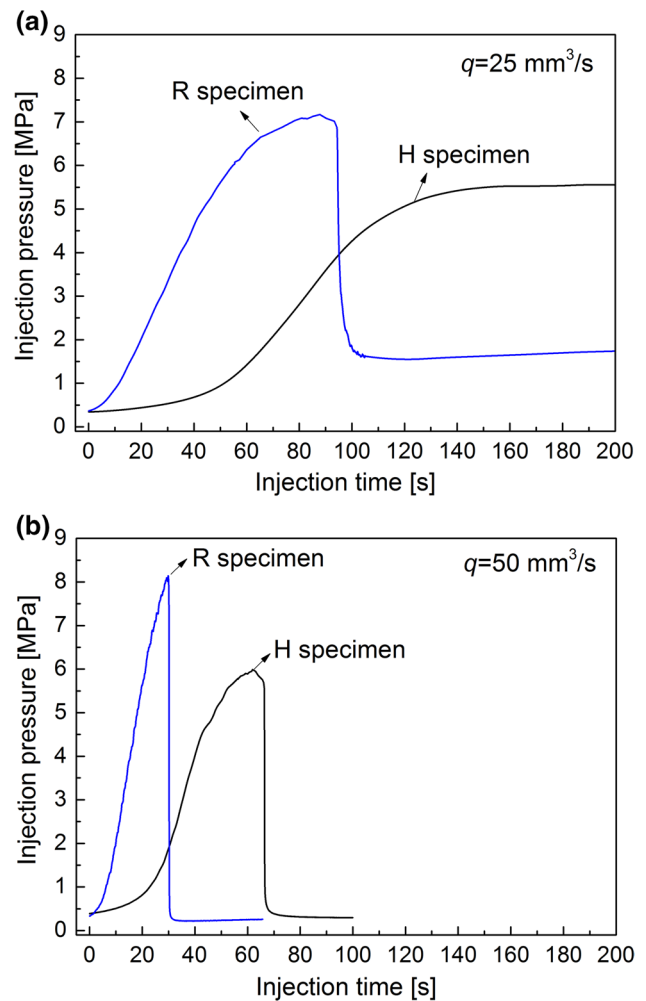


Fig. 6 Comparison of injection pressure–time curves for H and R specimens at injection rate of **a** $q = 25 \text{ mm}^3/\text{s}$ and **b** $q = 50 \text{ mm}^3/\text{s}$

fracturing behavior. Figure 6a, b compares typical injection pressure–time curves of H and R specimens at constant injection rates of 25 and 50 mm³/s, respectively. At the lower injection rate of 25 mm³/s, there was no breakdown for H specimen while breakdown occurred at 7.17 MPa for R specimen. When the injection rate was increased to 50 mm³/s, breakdown occurred in both R and H specimens with P_b of 8.14 and 6.00 MPa, respectively. These values are very close to the average BTS of rift plane and grain plane, which are 8.20 and 6.05 MPa. Under the stress conditions used here, tensile fractures will be generated in vertical direction. As a result, induced fractures will be along grain plane for R specimens, while they are along rift plane for H specimens. Therefore, it is confirmed that the difference in breakdown pressures comes from the difference in tensile strength between rift plane and grain plane.

Moreover, injection pressure developed more quickly in R specimens than that in H specimens, probably due to the influence of water infiltration along different permeability of media. As the specimens are hollow cylinders, water will mainly infiltrate radially outward from borehole. Each microcrack in granite represents a long narrow pore or a path available for water infiltration. The H specimens have two weak planes (rift and grain) in radial direction. Water will infiltrate into the rift plane faster compared to other directions because of its highest microcrack density, giving it the highest permeability. The R specimens, with grain and hardway planes in the radial direction, will have water mainly infiltrating in the grain plane or the hardway plane as the two have no significant difference in hydraulic conductivity. Overall, water infiltration speed will be the fastest when it occurs along the rift plane rather than the grain or hardway plane. As a result, at a given injection rate, injection pressure in H specimens developed more slowly than that in R specimens because of higher infiltration speed and greater water loss along the rift plane.

3.4 Sleeve Fracturing Test Results and Comparison

To exclude the influence of water infiltration, a set of sleeve fracturing tests as listed in Table 3 were performed on H specimens for comparison with hydraulic fracturing tests. Figure 7 shows comparisons of injection pressure–total injected volume curves at different injection rates of 1, 10, 50 and 100 mm³/s, respectively. Breakdown was observed in sleeve fracturing tests at both low and high injection rates. Ignoring the beginning part, injection pressure increased almost linearly until breakdown regardless of injection rate. Moreover, injection pressures developed much quicker in sleeve fracturing tests because there is no water loss during injection.

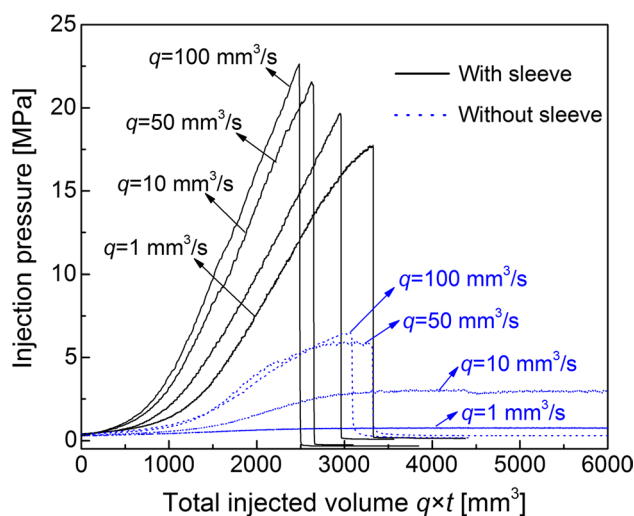


Fig. 7 Comparison of injection pressure variation between tests with and without sleeve

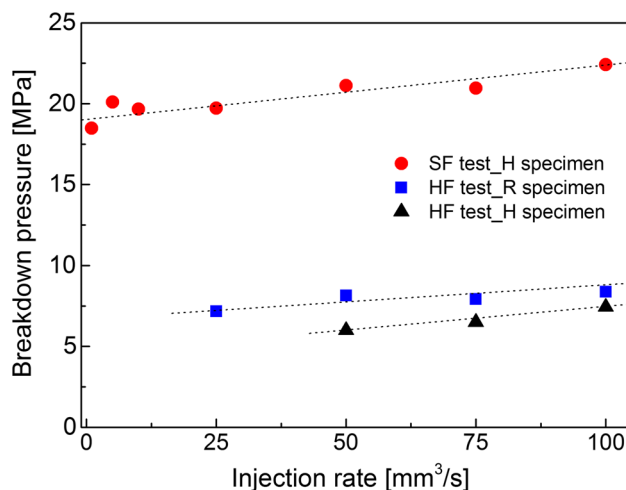


Fig. 8 Comparison of breakdown pressures under different test conditions. *SF* sleeve fracturing, *HF* hydraulic fracturing

3.5 Comparison of Breakdown Pressures

Figure 8 compares breakdown pressure P_b in the three sets of tests. Generally, P_b increases approximately linearly with increasing injection rate regardless of specimen or sleeve condition. In hydraulic fracturing tests, there is a threshold injection rate to induce breakdown, and this is expected to be between 25 and 50 mm³/s for H specimens and between 10 and 25 mm³/s for R specimens under the applied stress conditions in this study. The breakdown pressures for both H specimen and R specimen at the threshold injection rate are very similar to the average BTS of the cleavage planes where fractures were generated. However, it is still difficult to conclude that the BTS can well predict breakdown

pressure because breakdown pressure is still influenced by many other parameters, e.g., specimen size and borehole size. Guo et al. (1993) noted that the BTS predicts too low a breakdown pressure. Experimental results by Brenne et al. (2013) also show the inconsistency between the two for six types of rocks; particularly, the BTS of sandstone underestimated the breakdown pressures regardless of borehole size.

The P_b of H specimens in sleeve fracturing ranges around 18–23 MPa, which are more than two times higher than those in hydraulic fracturing. The classical breakdown prediction models mainly considering in situ stresses, tensile strength and pore pressure effect are not able to predict the anomalously high P_b . This phenomenon was also pointed out by Brenne et al. (2013), and they used the fracture mechanics model to explain the quite high breakdown pressures in sleeve fracturing test by assuming presence of cracks with relatively large length.

The granite specimen was split in two in all of sleeve fracturing tests by direct observation, while the induced fractures in hydraulic fracturing tests were usually along one side and in most cases fracture height was smaller than the specimen height based on CT observations. From the viewpoint of energy consumption, the energy released by sleeve fracturing must be higher, indicating a higher external work by the injection pressure. Figure 9 shows a typical example of injection pressure variation together with amplitude of induced acoustic emission (AE) hits detected during hydraulic fracturing test of H specimen at an injection rate of $100 \text{ mm}^3/\text{s}$. It is found that induced AE hits started at an injection pressure of near 7.0 MPa, which is very close to the BTS of rift plane of granite specimen. This indicated that cracks have likely been generated near borehole along rift plane when the injection pressure exceeds its tensile strength. However, with sleeve around borehole, there is no

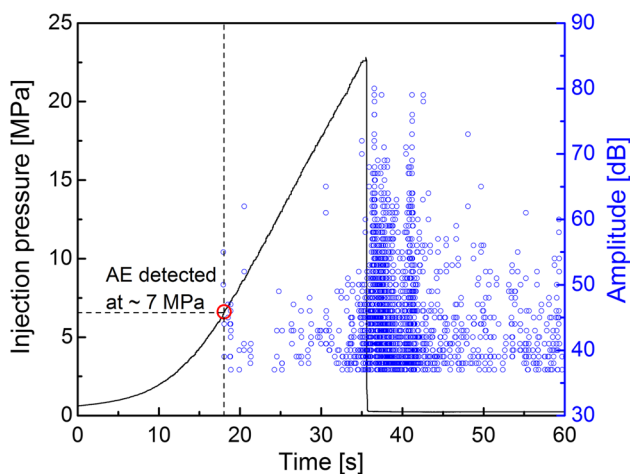


Fig. 9 Acoustic emission measurements in sleeve fracturing test at $q = 100 \text{ mm}^3/\text{s}$

water leaking into specimen and fluid pressure is not able to reach inside of the initial cracks to promote fracture propagation. Therefore, there is no decrease in injection pressure increment. Injection pressure continued to increase linearly because of the confined space of borehole until the specimen was totally fractured or the specimen failed. The resulted breakdown pressure is influenced by the stress gradient in the sample, which is specimen size dependent.

4 Analysis of Pressurization Rate Change

Pressurization rate is the variation of injection pressure per unit time. It is influenced by both specimen and injection rate. The typical injection pressure–time curve in hydraulic fracturing tests can be divided into a linear section and a nonlinear section ignoring the very beginning section. The slope of the linear section is noted as resultant pressurization rate, and its estimated value under each test condition is given in Tables 2 and 3. For both hydraulic and sleeve fracturing tests, the resultant pressurization rate increases with increasing injection rate, but not in a linear fashion, especially in hydraulic fracturing tests. The resultant pressurization rates in sleeve fracturing tests are obviously much higher than those in hydraulic fracturing test.

The nonlinear section starting from a point where injection pressure deviates from the linear approximation to the point where injection pressure starts to decrease or converges is fitted by a quadratic polynomial, and dP/dt was calculated through time integration. To distinguish it from the resultant pressurization rate estimated from the linear section, dP/dt is defined as “pressurization increment.”

Figure 10 plots the pressurization increment with respect to injection pressure for H specimens at different injection rates of $10\text{--}100 \text{ mm}^3/\text{s}$. For hydraulic fracturing tests, the pressurization increment initially decreases almost linearly with increasing injection pressure regardless of injection rate. It then deviates from the linear approximation at a certain point, P_i . Magnitude of the injection pressure at point P_i is noted beside each curve. The ratio of P_i and the maximum injection pressure P_{\max} or P_b is around 78–89%. The pressurization increment decreases due to loss of injection fluid, as the inflow is constant (because injection rate is constant) while outflow increases. dP/dt reduces to almost zero when the inflow and outflow are balanced. When water infiltration is ignored in sleeve fracturing tests, injection pressure–time curve is almost linear and pressurization rate is nearly constant until the breakdown.

A similar phenomenon has been reported by Song and Haimson (2000, 2001), who found two different types of dP/dt variation with injection pressure in Berea sandstone and Tablerock sandstone having high porosities of 17–25 and 26.0%, respectively. When the injection rate was too low

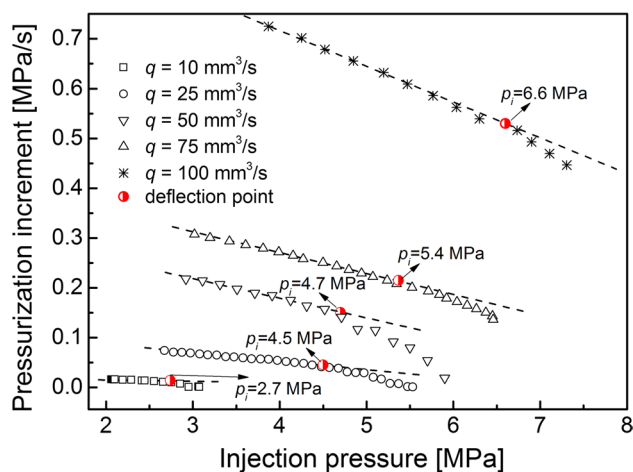


Fig. 10 Pressurization increment dP/dt with respect to injection pressure at different injection rates for H specimens in hydraulic and sleeve fracturing tests. P_i is the injection pressure at which pressurization rate deviates from the linear approximation

to pressurize the wellbore for hydrofracturing, dP/dt linearly decreased with increasing injection pressure all the way to zero, while for a high injection rate, dP/dt showed a linear decrease at first and then it deviated from the linear approximation and became even faster slow down at a certain point. The point was defined as the “apparent breakdown pressure,” where permeability suddenly changes due to tensile fracturing.

However, unlike Tablerock sandstone, granite showed a nonlinear variation of pressurization increment at both low and high injection rates. This is probably due to differences in pore structures between the porous sandstones and the low-permeability granite. Zimmerman (1991) noted that the pore compressibility of any non-circular pore must be greater than that of a circular pore. There are many thin and long microcracks in granite, and they could open even with a small injection pressure. This could result in dilation of granite specimen and permeability increase from an early stage of injection. Song et al. (2004) found that the permeability of Westerly granite increases with decreasing effective pressure hence increasing pore pressure. The pores in the two sandstones are much less compressible and show negligible deformation at the early pressure stage. The permeability of the sandstones changed at the late stage owing to induced fractures.

5 X-ray CT Observations on Induced Fractures

After the hydraulic fracturing test specimen was removed. CT scan was then performed on the specimen to observe internal changes, particularly induced fractures. Figures 10

and 11 show typical two-dimensional CT images of cross sections of H and R specimens after testing. The resolution is 0.0569 mm/pixel.

Figure 11a–c compares the induced fractures in H specimens at different injection rate of $q = 50, 75$ and $100 \text{ mm}^3/\text{s}$, respectively. Figure 12a–d compares the induced fractures in R specimens at different injection rate of $q = 25, 50, 75$ and $100 \text{ mm}^3/\text{s}$, respectively. It is confirmed that fractures are along the rift plane for H specimens and they are along the grain plane for R specimens. In most cases, fractures are located on one side rather than being symmetrically distributed around the borehole. The main reasons for the result are that the borehole is not exactly in the center of specimen and the granite specimen is heterogeneous and anisotropic. Moreover, in most cases fractures were generated only in the upper part or the lower part of specimen, which means the height of fractures is usually smaller than the height of specimen.

Note that one H specimen showed no peak in the pressure–time curves at $q = 25 \text{ mm}^3/\text{s}$, indicating the absence of breakdown. However, a few very thin fractures with aperture < 1 pixel were observed in enlarged image of the specimen. At low injection rates and relative low injection pressures compared to the breakdown pressure, water slowly infiltrates granite specimen. It is likely that preexisting microcracks in granite opened and extended and further connected each other to form longer cracks.

The aperture of induced fractures was roughly measured by enlarging the CT images in the open source software of ImageJ (Ferreira and Rasband 2012) and counting the number of pixels along the direction of fracture width based on the intensity values of pixels, as the intensity values of pixels indicating the induced fracture, which is empty space, is much lower than those of pixels indicating the granite. The accuracy was limited to 1 pixel. The maximum aperture of fractures was decided by comparing measurements in different slices corresponding to different heights of the specimen. Table 2 lists the results of the maximum aperture of fractures under different test conditions. Generally, the aperture increases with increasing injection rate or increasing breakdown pressure. Moreover, at the same injection rate in hydraulic fracturing tests, the R specimens showed apertures 1–3 pixels larger than those in the H specimens. This is because the breakdown pressures were higher in the R specimens.

The fractures were extracted to show their 3D geometries and apertures. Figure 13a–d compares four typical cases of two H specimens and two R specimens with injection rates of 50 and $100 \text{ mm}^3/\text{s}$, respectively. Coincidentally, the two cases at $q = 50 \text{ mm}^3/\text{s}$ show clear fracture branching. One started from the borehole, while the other started in the middle of specimen. It is highly likely that the two branching are both related to quartz clusters inside the specimen. The

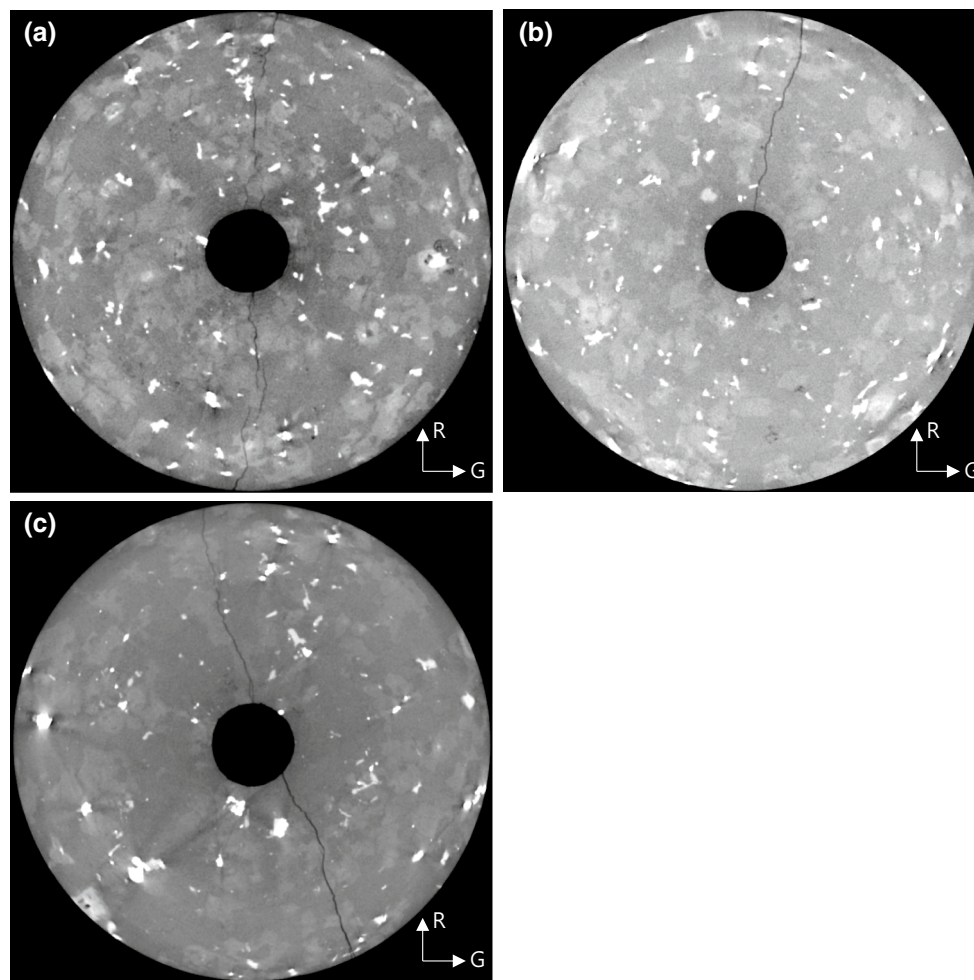


Fig. 11 Comparison of induced fractures in H specimens at various injection rates **a** $q = 50 \text{ mm}^3/\text{s}$, **b** $q = 75 \text{ mm}^3/\text{s}$ and **c** $q = 100 \text{ mm}^3/\text{s}$

quartz grains have abundance of microcracks, which can be classified into intragranular, intergranular and boundary ones (Diaz et al. 2016). These different types of microcracks influence how fractures were generated. Further study is needed in this regard. Tortuosity, which is defined as the ratio of the total length of a fracture and the distance between its two ends, was measured on the main fractures ignoring the branching. The four cases in Fig. 13a–d gave a result of 1.055, 1.056, 1.044 and 1.056, respectively. There is almost no difference among the values.

Figure 14 shows typical images of induced fractures in sleeve fracturing tests at injection rates of 50 and 100 mm^3/s . Specimens were split in two and the fracturing was accompanied by a clearly audible sound, indicating high energy release. Preliminary acoustic emission measurement showed that the maximum acoustic amplitudes detected in sleeve fracturing test was around 80 dB on average which is 1.1–1.3 times higher than those in hydraulic fracturing tests under the same injection rate of 100 mm^3/s . Moreover, the induced fractures in sleeve fracturing tests appear to be straighter

with less branching than those in hydraulic fracturing tests. The measured tortuosity is 1.049 for $q = 50 \text{ mm}^3/\text{s}$ and 1.038 for $q = 100 \text{ mm}^3/\text{s}$. There is only tiny difference between tortuosities of hydraulic and sleeve fracturing tests probably due to a limited size of specimen.

6 Discussions

Pocheon granite is generally considered impermeable due to its very low permeability. However, many long and partially connected microcracks exist inside granite especially in the three cleavage planes of rift, grain and hardway. Injected fluid can infiltrate the rock matrix and open these microcracks under the action of injection pressure. Comparisons of hydraulic and sleeve fracturing test results showed that water infiltration significantly influences hydraulic fracturing behavior of granite. Three important things arise from the test results and require further discussion.

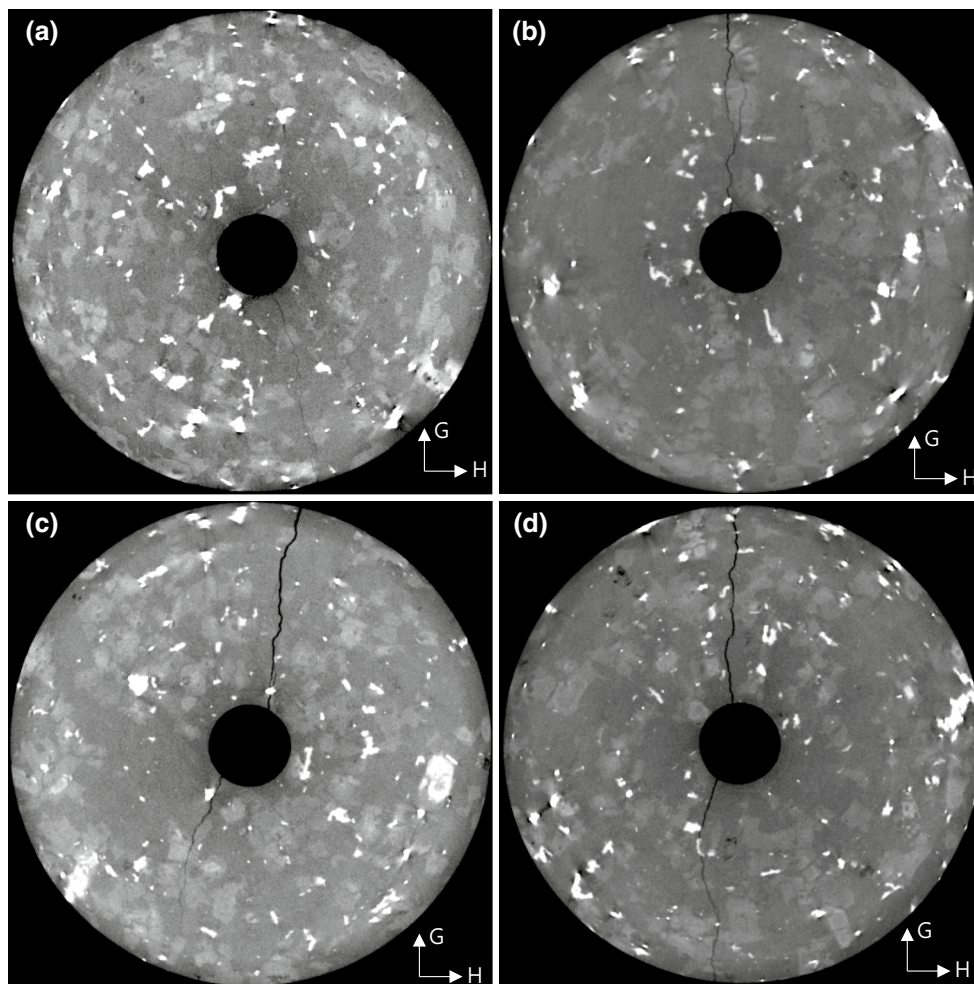


Fig. 12 Comparison of induced fractures in R specimens at various injection rates **a** $q = 25 \text{ mm}^3/\text{s}$, **b** $q = 50 \text{ mm}^3/\text{s}$, **c** $q = 75 \text{ mm}^3/\text{s}$ and **d** $q = 100 \text{ mm}^3/\text{s}$

1. Hydraulic fracturing behavior of granite is different from that of other rocks such as sandstone due to abundant preexisting natural microcracks inside granite. This implies that water infiltration influence is different for different pore structures in rocks. However, Zoback and Byerlee (1975) noted that though microcracks dilatancy has influences on permeability of Westerly granite specimens in laboratory, the magnitude of permeability contributed by microcracks measured in laboratory is much less than that of in situ conditions. Dilatancy and fluid flow occur on the scale of joints and fractures in field scale. Nevertheless, the finding on the effect of microcracks can be a reference for studying influence of large scale natural fractures.
2. Although granite shows mild anisotropy due to existing of the three cleavages compared to sedimentary rocks, the influence of the anisotropy on hydraulic fracturing behavior was clearly confirmed at a core scale. However, when it comes to the field scale with complex geological structures which were not able to be reflected by core-scale samples in laboratory, the anisotropy effect may not be as prominent as in the laboratory scale. For example, Duevel and Haimson (1997) noted that the pink Lac du Bonnet granite is practically isotropic in compression despite that its tensile strength and tensile modulus show stronger anisotropy. The influence of anisotropy in Pocheon granite will be further investigated on larger samples considering in situ stresses.
3. The estimation of pressurization increment inferred that some local damages (cracks or fractures) inside specimen may have already happened at around 78–89% of the maximum injection pressure or the breakdown pressure. Therefore, we anticipate that a specimen is likely to achieve breakdown at a relatively lower injection pressure through cyclic injection (Zhuang et al. 2016a, 2017). This might reduce the induced seismicity during hydraulic stimulation, as preliminary experimental results show that the maximum amplitude of induced AE

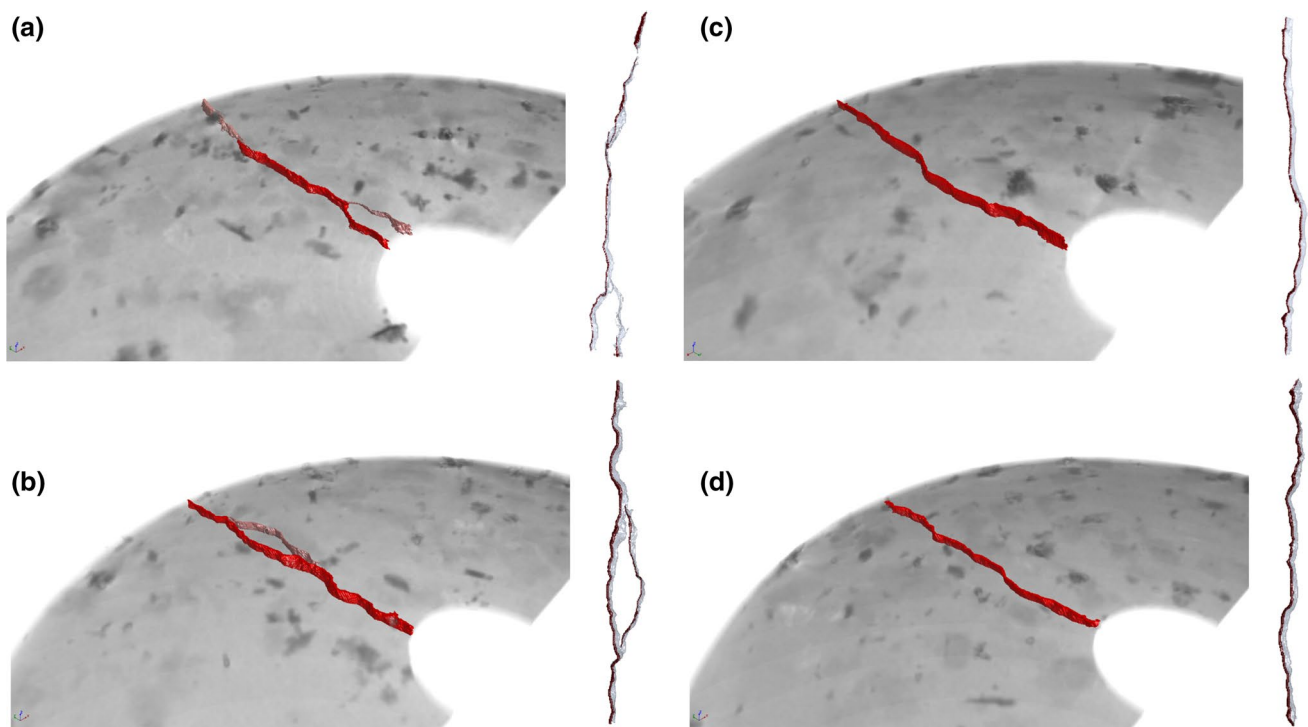


Fig. 13 Extraction of main fractures show 3D geometry and front view **a** $q = 50 \text{ mm}^3/\text{s}$, H specimen, **b** $q = 50 \text{ mm}^3/\text{s}$, R specimen, **c** $q = 100 \text{ mm}^3/\text{s}$, H specimen and **d** $q = 100 \text{ mm}^3/\text{s}$, R specimen

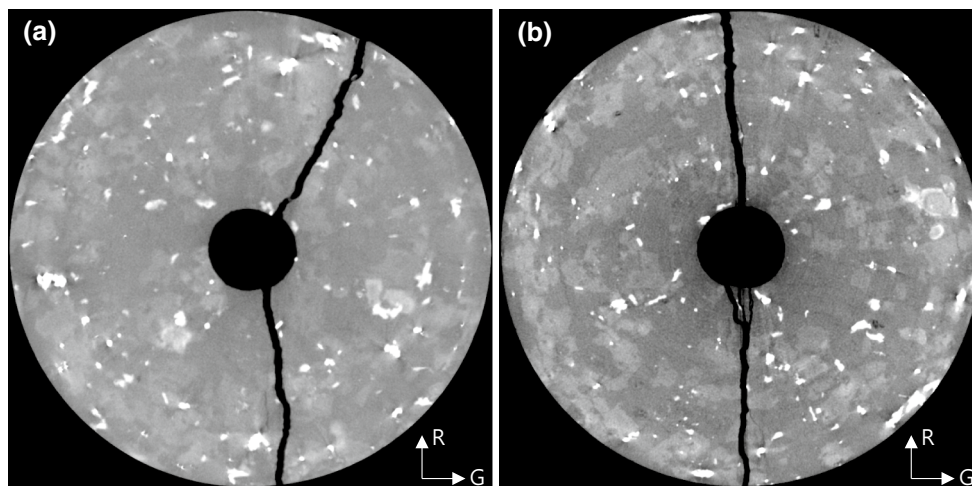


Fig. 14 Induced fractures in sleeve fracturing tests at injection rates of **a** $q = 50 \text{ mm}^3/\text{s}$ and **b** $q = 100 \text{ mm}^3/\text{s}$

was reduced by cyclic injection with lowered injection pressure (Zhuang et al. 2017). Further study is needed in this field.

Note that all of the test results in this study are limited to the condition of zero confining pressure. Confining pressure, shear stresses as well as other factors such as temperature will influence permeability of granite samples (Morrow et al. 1986; Song et al. 2004; Alam et al. 2015). As a result, water

infiltration varies at different in situ conditions. In this study, the stress condition was set to be very simple and ideal. Fluid infiltration and induced fracture mainly happened along the weak planes with a number of microcracks. When considering in situ stresses and natural fractures for field application, fluid infiltration will become more complex. From this respect, the experimental findings in the laboratory have to be used as basic study for application of hydraulic fracturing that will occur in a more complex manner in field.

7 Conclusions

A series of hydraulic and sleeve fracturing tests were performed on granite specimens taking into account anisotropy. Effect of injection rate varying from 1 to 100 mm³/s was investigated. Injection pressure–time curves were classified into two types with and without fracturing corresponding to low and high injection rates.

1. The maximum injection pressure or the breakdown pressure increases with increasing injection rate. There is a threshold injection rate in hydraulic fracturing tests at which breakdown can be induced. Injection rates below the threshold caused the injection pressure to develop too slowly to break the granite specimen. Injection pressure stops increasing when the specimen reaches a saturation state at which inflow equals outflow. If the injection rate is too high, injection pressure develops quickly and there is not enough time for water to fully infiltrate the specimen. In such a case, specimen failed at a relatively high breakdown pressure.
2. Hydraulic fracturing behavior of granite is quite different from sleeve fracturing where water infiltration is excluded. Injection pressure develops nonlinearly in hydraulic fracturing tests before reaching the maximum value, while it develops approximately linearly in sleeve fracturing tests. Without confining pressure, the breakdown pressures in hydraulic fracturing are similar to the BTS, while they are more than two times higher than the BTS in sleeve fracturing.
3. Cleavage anisotropy has influence on the orientation of generated fractures. Induced fractures are mainly along rift plane for H specimens and they are along grain plane for R specimens. The difference of breakdown pressures between the two specimens compared at the same injection rate is very close to the difference in the BTS between rift plane and grain plane.
4. X-ray CT observations show that the maximum aperture of induced fractures increases with increasing breakdown pressure in hydraulic fracturing test. Tortuosities of generated fractures were measured to be around 1.04–1.06. There is no obvious difference among different test conditions. The limited specimen size could be one important reason.

Acknowledgements This work has been supported by the International Research Program of Korea Institute for Advancement of Technology (KIAT) under grant agreement No. N0002098, in the framework of the European Union's Horizon 2020 Research and Innovation Programme under grant agreement No. 691728. We thank Dr. Insun Song for his valuable discussions on the experimental data analysis. We also highly appreciate all the comments from the three anonymous reviewers.

Open Access This article is distributed under the terms of the Creative Commons Attribution 4.0 International License (<http://creativecommons.org/licenses/by/4.0/>), which permits unrestricted use, distribution, and reproduction in any medium, provided you give appropriate credit to the original author(s) and the source, provide a link to the Creative Commons license, and indicate if changes were made.

References

- Alam AKMB, Fujii Y, Fukuda D, Kodama J, Kaneko K (2015) Fractured rock permeability as a function of temperature and confining pressure. *Pure Appl Geophys* 172:2871–2889
- Bertels SP, DiCarlo DA, Blunt MJ (2001) Measurement of aperture distribution, capillary pressure, relative permeability, and in situ saturation in a rock fracture using computed tomography scanning. *Water Resour Res* 37(3):649–662
- Brenne S, Molenda M, Stoeckert F, Alber M (2013) Hydraulic and sleeve fracturing laboratory experiments on 6 rock types. *Open Access* 10(5772/56301):425–436
- Chen Y, Nagaya Y, Ishida T (2015) Observations of fractures induced by hydraulic fracturing in anisotropic granite. *Rock Mech Rock Eng* 48:1455–1461
- Degue KM, Ladanyi B (2000) Effect of fluid penetration and pressurizing rate on hydraulic fracturing. In: Girard, Liebman, Breeds, Doe (eds) *Pacific Rocks 2000*, Balkema, Rotterdam, pp 181–188
- Detournay E, Cheng A (1992) Influence of pressurization rate on the magnitude of the breakdown pressure. In: Tillerson JR, Wawersik WR (eds) *Rock mechanics*. Balkema, Rotterdam, pp 325–333
- Diaz MB, Jung SG, Zhuang L, Kim KY, Yeom S, Shin HS (2016) Effect of cleavage anisotropy on hydraulic fracturing behavior of Pocheon granite. In: *Proceedings of the 50th US rock mechanics/geomechanics symposium*, Houston, ARMA, pp 16–143
- Douglass PM, Voight B (1969) Anisotropy of granites: a reflection of microscopic fabric. *Geotechnique* 19:376–398
- Duevel B, Haimson B (1997) Mechanical characterization of pink Lac Du Bonnet granite: Evidence of nonlinearity and anisotropy. *Int J Rock Mech Min Sci* 34:3–4, Paper No. 117
- Ferreira T, Rasband W (2012) *ImageJ User Guide-IJ1.46r*
- Fujii Y, Takemura T, Takahashi M, Lin W (2007) Surface features of uniaxial tensile fractures and their relation to rock anisotropy in Inada granite. *Int J Rock Mech Min Sci* 44(1):98–107
- Garagash D, Detournay E (1996) Influence of pressurization rate on borehole breakdown pressure in impermeable rocks. In: Aubertin, Hassani, Mitri (eds) *Rock mechanics*, Balkema, Rotterdam
- Guo F, Morgenstern NR, Scott J (1993) Interpretation of hydraulic fracturing breakdown pressure. *Int J Rock Mech Min Sci Geomech Abstr* 30(6):617–626
- Ha SJ, Yun TS, Kim KY, Jung SG (2017) Experimental study of pumping rate effect on hydraulic fracturing of cement paste and mortar. *Rock Mech Rock Eng* 50:3115–3119
- Haimson BC (1968) Hydraulic fracturing in porous and nonporous rock and its potential for determining in situ stresses at great depth. Ph.D. Thesis, University of Minnesota, USA
- Haimson B (1975) The state of stress in the earth's crust. *Rev Geophys Space Phys* 13(3):350–352
- Haimson BC (1999) Six hydraulic fracturing campaigns at the URL, Manitoba. In: *Proceedings of 9th ISRM congress*, 25–28 August, Paris
- Haimson B, Doe TW (1983) State of stress, permeability, and fractures in the Precambrian granite of Northern Illinois. *J Geophys Res* 88(B9):7355–7372
- Haimson B, Fairhurst C (1967) Initiation and extension of hydraulic fractures in rocks. *Soc Pet Eng J* 7:310–318

- Haimson B, Fairhurst C (1969) Hydraulic fracturing in porous-permeable materials. *J Pet Technol* 21:811–817
- Haimson B, Fairhurst C (1970) In-situ stress determination at great depth by means of hydraulic fracturing. In: Somerton WH (ed) *Rock mechanics-theory and practice. The proceedings of the 11th symposium on rock mechanics, 16–19 June 1969, Berkeley*, pp 559–584
- Haimson BC, Lee CF (1980) Hydrofracturing stress determination at Darlington, Ontario. In: *Proceedings of 13th Canadian symposium on rock mechanics, Canadian Institute of Mining and Metallurgy*, pp 42–50
- Haimson BC, Zhao Z (1991) Effect of borehole size and pressurization rate on hydraulic fracturing breakdown pressure. In: Roegiers JC (ed) *Rock mechanics as a multidisciplinary science. Balkema, Rotterdam*, pp 191–199
- Hubbert KM, Willis DG (1957) Mechanics of hydraulic fracturing. *Petrol Trans AIME* 210:153–168
- Ishida T, Chen Q, Mizuta Y (1997) Effect of injected water on hydraulic fracturing deduced from acoustic emission monitoring. *Pure Appl Geophys* 150:627–646
- Ishida T, Sasaki S, Matsunaga I, Chen Q, Mizuta Y (2000) Effect of grain size in granitic rocks on hydraulic fracturing mechanism. In: *Proceedings of sessions of geo-denver 2000, trends in rock mechanics, geotechnical special publication No. 102, ASCE*, pp 128–139
- Ishida T, Chen Q, Mizuta Y, Roegiers JC (2004) Influence of fluid viscosity on the hydraulic fracturing mechanism. *J Energy Resour Technol* 126:190–200. <https://doi.org/10.1115/1.1791651>
- Ishida T, Aoyagi K, Niwa T, Chen Y, Murata S, Chen Q, Nakayama Y (2012) Acoustic emission monitoring of hydraulic fracturing laboratory experiment with supercritical and liquid CO₂. *Geophys Res Lett*. <https://doi.org/10.1029/2012gl052788>
- Jia L, Chen M, Sun L, Sun Z, Zhang W, Zhu Q, Sun Z, Jin Y (2013) Experimental study on propagation of hydraulic fracture in volcanic rocks using industrial CT technology. *Pet Explor Dev* 40(3):405–408
- Johns RA, Steude JS, Castanier LM, Roberts PV (1993) Nondestructive measurements of fracture aperture in crystalline rock cores using X ray computed tomography. *J Geophys Res* 98(B2):1889–1900
- Keller AA (1997) High resolution CAT imaging of fractures in consolidated materials. *Int J Rock Mech Min Sci* 34(3/4): 358, Paper No. 155
- Li X, Duan Y, Li S, Zhou R (2017) Study on the progressive failure characteristics of Longmaxi shale under uniaxial compression conditions by X-ray micro-computed tomography. *Energies* 10(303):1–13
- Morgan SP, Li BQ, Einstein HH (2017) Effect of injection rate on hydraulic fracturing of Opalinus clay shale. In: *Proceedings of the 51st US Rock mechanics/geomechanics symposium, San Francisco, California, ARMA 17–873*
- Morrow CA, Zhang BC, Byerlee JD (1986) Effective pressure law for permeability of Westerly granite under cyclic loading. *J Geophys Res* 91(B3):3870–3876
- Park DW, Kim HC, Lee CB, Hong SS, Chang SW, Lee CW (2004) Characteristics of the rock cleavage in Jurassic granite, Pocheon. *J Pet Soc Korea* 13(3):133–141 (in Korean)
- Renard F, Bernard D, Desrues J, Ougier-Simonin A (2009) 3D imaging of fracture propagation using synchrotron X-ray microtomography. *Earth Planet Sci Lett* 286(1–2):285–291
- Solberg P, Lockner D, Byerlee JD (1977) Shear and tension hydraulic fractures in low permeability rocks. *Pure Appl Geophys* 115(1):191–198
- Solberg P, Lockner D, Byerlee JD (1980) Hydraulic fracturing in granite under geothermal conditions. *Int J Rock Mech Min Sci Geomech Abstr* 17(1):25–33
- Song I, Haimson B (2000) Hydraulic fracturing experiments in highly porous Berea sandstone. In: Girard, Liebman, Breeds, Doe (eds) *Proceedings of Pacific rocks 2000*, pp 1185–1192
- Song I, Haimson B (2001) Effect of pressurization rate and initial pore pressure on the magnitude of hydrofracturing breakdown pressure in Tablerock sandstone. *Rock Mechanics in the National Interest, Elsworth, Tinucci & Heasley (eds), A.A. Balkema*, pp 235–242
- Song I, Elphick SC, Main IG, Ngwenya BT, Odling NW (2004) One-dimensional fluid diffusion induced by constant-rate flow injection: theoretical analysis and application to the determination of fluid permeability and specific storage of a cored rock sample. *J Geophys Res* 109(B05207):1–13. <https://doi.org/10.1029/2003JB002395>
- Stoekchert F, Molenda M, Brenne S, Alber M (2015) Fracture propagation in sandstone and slate—laboratory experiments, acoustic emissions and fracture mechanics. *J Rock Mech Geotechn Eng* 7:237–249
- Zeng Z, Roegiers JC (2002) Experimental observation of injection rate influence on the hydraulic fracturing behavior of a tight gas sandstone. *SPE/ISRM Rock Mechanics Conference, Irving, Texas, SPE/ISRM 78172*
- Zhao Z, Kim H, Haimson B (1996) Hydraulic fracturing initiation in granite. In: Aubertin, Hassani, Mitri (eds) *Rock mechanics, Balkema, Rotterdam*, pp 1279–1284
- Zhuang L, Kim KY, Jung SG, Nam YJ, Min KB, Park S, Zang A, Stephansson O, Zimmermann G, Yoon JS (2016a) Laboratory study on cyclic hydraulic fracturing of Pocheon granite. In: *Proceedings of the 50th US rock mechanics/geomechanics symposium, Houston, ARMA 16–163*
- Zhuang L, Diaz MB, Jung SG, Kim KY (2016b) Cleavage dependent indirect tensile strength of Pocheon granite based on experiments and DEM simulation. *J Korean Soc Rock Mech Tunn Undergr Space* 26(4):316–326
- Zhuang L, Kim KY, Jung SG, Nam YJ, Min KB, Park S, Zang A, Stephansson O, Zimmermann G, Yoon JS (2017) Laboratory evaluation of induced seismicity reduction and permeability enhancement effects of cyclic hydraulic fracturing. In: *Proceedings of the 51st US rock mechanics/geomechanics symposium, San Francisco, California, ARMA 17–757*
- Zimmerman RW (1991) *Compressibility of sandstones*, 1st edn. Elsevier Science Publishers B.V., Amsterdam
- Zoback MD, Byerlee JD (1975) The effect of microcrack dilatancy on the permeability of Westerly granite. *J Geophys Res* 80:752–755
- Zoback MD, Rummel F, Jung R, Raleigh CB (1977) Laboratory hydraulic fracturing experiments in intact and pre-fractured rock. *Int J Rock Mech Min Sci Geomech Abstr* 14:49–58